FLEXIBLE ELECTROMAGNETIC ACTUATORS FOR WEARABLE HAPTIC DEVICES

Naji Tarabay[1], Ananya Renuka Balakrishna[2], Tianshu Liu[3], Priyanshu Agarwal[3], and Camilo Velez[1]
[1]University of California, Irvine, USA
[2]University of California, Santa Barbara, USA
[3]Reality Labs Research, Meta Platforms Inc., Washington, USA

ABSTRACT

Electromagnetic actuators play a crucial role in virtual reality and haptic devices, providing precise mechanical movements to convey realistic sensations, enhancing immersion and presence, and enabling new applications that blur the boundaries between the physical and virtual worlds. This work presents a new type of soft electromagnetic haptic actuators combining sub-mm resolution Digital Light Processing (DLP) multimaterial 3D printing of flexible membranes with NdFeB magnets and planar coils. A study varying fabrication parameters and commercial components for the actuator was conducted, yielding a device that can achieve 12-47 µm vertical displacement with 160-340 mW maximum input power at 200 Hz (resonance), in a form factor 12 mm x 12 mm x 2.8 mm. The prototyped actuators offer a venue to develop a new class of soft haptic actuators with high performance, low power consumption, ease of integration with wearables, high displacement, and small form factor.

KEYWORDS

Electromagnetic, actuators, haptic, digital light processing, flexible.

INTRODUCTION

Virtual environments can unlock new realms of sensations and experiences that were previously inaccessible due to physical limitations, financial constraints, or technological barriers, vastly expanding the boundaries of human exploration and interaction [1]. Skin-integrated haptic actuators, primarily employing soft electromagnetic actuation, are of great interest in advancing wearable haptic devices for virtual and augmented reality (VR/AR) platforms [2,3]. To create a truly immersive VR/AR experience, the integration of the virtual and physical environment must provide user feedback and intuitive interface sufficiently consistent with expectations of reality [4]. However, current soft actuators for haptics applications meet several limitations in real life applications, including slow response [5], low force output [6], high-control voltages [7,8], and bulky sizes [9,10]. These limitations restrict their importance in untethered wearable devices. For example, while dielectric elastomer actuators exhibit a good mechanical performance [11,12], their high actuation voltage that typically exceeds thousands of volts raises safety concerns for human use. On the other hand, pneumatic fluidic actuators are commonly used in soft robotics and haptic actuators due to their ability to generate large force output [13]; however, this type of actuators need high-pressure equipment, typically exceeding 300 kPa and are slow in response (<0.5 Hz) [14]. Compared to current soft functional actuators, conventional electromagnetic actuators still offer many advantages such as fast response and lower actuation voltage, as well as highly programmable and well-controlled movements. Electromagnetic actuators are considered a vital component in wearable haptic devices for VR/AR platforms [15], enabling users to feel tactile sensations and feedback in real-time. By providing vibrations, forces, and displacements, these actuators create a more immersive and engaging feedback, making virtual and augmented reality experiences more natural and intuitive.

In this work, we present a new design of multimaterial 3D printed soft electromagnetic actuator. We combine permanent magnets with flexible resins acting as displacing membranes and rigid resins for structural integrity using sub-mm pixel size Digital Light Processing (DLP) 3D printing technique. The proposed fabrication technique was used to prototype magnetic actuators for haptic applications offering a venue to develop a new class of cost effective soft haptic actuators with high performance, low power consumption, ease of integration with wearable devices, high displacement, and smaller form factor than commercially available alternatives.

EXPERIMENTAL METHODS

Design Concept and Operating Principle

Electromagnetic actuators operate under fundamental principles of electromagnetic forces translated into mechanical work. A planar coil placed below a permanent magnet surrounded by a flexible membrane, as shown in Fig. 1a. When an electric current flows through the coil it induces a magnetic field (Biot–Savart law), generating repelling/attractive forces to the permanent magnet (according to the magnet's magnetization direction and the current direction).

A lumped element model of such actuators is typically described as the composition of two domains (electromagnetic and mechanical) represented by an electrical circuit (a coil with equivalent inductance and resistance), and the mechanical circuit (a mass, spring, damper). The coupling between two domains is the resulting magnetic force directly proportional to the electric current (Faraday's laws of electromagnetic induction). Therefore, to model the system, we need an expression to model magnetic forces.

The differential element of force dF between the permanent magnet and each differential segment of coil dl can be calculated by integrating the standard magnetic force formula $dF = Idl \times B$ where B is the magnetic flux density due to the magnet and I is the total current in the coil (the Lorentz force law).

We will use cylindrical coordinates (ρ, φ, z) with origin at the center of a magnet. If the magnet is defined as a magnetic dipole by $m = (VB_r/\mu_0)\hat{z}$ (in units of $A \cdot m^2$) where B_r is the residual flux density expressed in Tesla, V is the volume of the magnet, and μ_0 is the permeability of vacuum. If the point in the space is defined as $r = R\hat{\rho} - z\hat{z}$, then the magnetic flux density $(B(r))$ at r can be simplified using the following equation [16]:

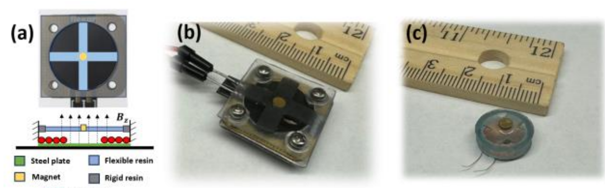

Figure 1: (a) Working principle of the electromagnetic haptic actuator. (b)(c) Two proposed prototypes of 3D printed actuators varying commercial coils.

978-1-940470-05-4/HH2024/$25©2024TRF
DOI 10.31438/TRF.HH2024.97

$$B(r) = \frac{VB_r}{4\pi(R^2+z^2)^{\frac{3}{2}}}\left[-\frac{3zR}{R^2+z^2}\hat{\rho} + \left(\frac{3z^2}{R^2+z^2} - 1\right)\hat{z}\right]. \qquad (1)$$

The total force F is calculated by integrating dF form 0 to $2\pi N$ over φ, where N is the number of turns for the coil. With the replacement $\beta = z/R$, the radial component will cancel because of the symmetry, resulting in:

$$F = \frac{3\mu_0 mNI}{2R^2}\frac{\beta}{(1+\beta^2)^{\frac{5}{2}}}\hat{z}, \qquad (2)$$

A magnet embedded in the membrane will experience this force making the membrane deflect. The displacement of the membrane is then given by $\Delta d = F/k$, where k denotes the effective stiffness of the membrane. Thus, the force applied to the membrane acts as if it were a central load. The stiffness of a centrally loaded circular membrane with clamped edges can be calculated by [17]:

$$k = \frac{16\pi E h^3}{3d^2(1-v^2)}, \qquad (3)$$

where E, h, d, and v represent Young's modulus of the membrane, membrane's thickness, membrane's diameter, and Poisson ratio of the membrane, respectively.

Sinusoidally Driven Systems: Second Order DE's

The mechanical domain can be modeled as a damped forced harmonic oscillator. If we define the oscillator as a mechanical system with mass m_m, damping coefficient b, spring constant k, and subject to a sinusoidal driving force $|F|cos(\omega t)$ (with constant amplitude $|F|$), then the governing differential equation (DE) for the system is:

$$m_m\frac{d^2x}{dt} + b\frac{dx}{dt} + kx = |F|cos(\omega t), \qquad (4)$$

The gain, represented by the ratio of output amplitude to input amplitude in the real equation, is explicitly expressed as:

$$g = g(w) = \frac{1}{\sqrt{(k-m_m w^2)^2 + b^2 w^2}}. \qquad (5)$$

Values for m_m can be measured, k can be calculated according to equation (3), and b is extracted from bode plot measure according to $b = 1/Q \cdot \sqrt{(mk)}$ where $Q = f_N/\Delta f$. Q is the quality factor, f_N is the natural frequency, and Δf is the difference between the frequencies at which the amplitude is equal to $0.707A_N$, where A_N is the amplitude at f_N. Values for m, b, and k are found to be 99 mg, 0.031 Ns/m, and 11.8 N/m.

Fabrication Process

The fabrication process incorporates a 3 mm diameter, 1 mm thick magnet of N52 grade (from Supermagnetman), embedded in a 500 µm thick flexible printed membrane over the planar coil as shown in Fig. 1b-c. Hard resin was added at the edges of the membrane for mechanical stability. Seven different prototypes were fabricated to increase displacement and decrease power consumption evaluating the following design changes: (1) Commercial Planar coil. Three coils were evaluated: 12-layers rigid PCB (prototypes 1, 2, 3, and 4) and flexible single-layer PCB (prototypes 5 and 6) from Microbots.io (both represented in Fig. 1b), and winded WR121210-27M8-ID coils (prototype 7) from TDK (Fig. 1c) of diameters 20, 20, and 12 mm respectively. (2) Membrane resins from Liqcreate ("Flexible-X" and "Premium Flex"), 2.4 and 1.9 MPa Young's modulus respectively. (3) Steel plate addition to the back of the coils, to concentrate the magnetic flux density and maximize the displacement.

The membrane was fabricated using a DLP printing process (Anycubic Photon Mono 4K printer), which uses an LED projector to cure liquid resin layer by layer. The first step involves printing the hard resin in the exterior, using a layer thickness of 100 µm. Each layer was cured for 8 seconds, except for the two bottom layers, which were cured for 70 seconds to ensure a strong foundation. Printer parameters such as lift speed was set at 90 mm/min, while the retract speed was 240 mm/min, allowing for precise control over the printing process. The second step in the fabrication process involves printing the flexible resin in the interior, with a layer thickness of 100 µm. Each layer was cured for 5 seconds, except for the two bottom layers, which were cured for 40 seconds. The printing process was precisely controlled, with a lift speed of 90 mm/min and a retract speed of 240 mm/min. Post printing steps involve washing with isopropyl alcohol (91%) for 5 minutes, 10 minutes air drying.

Finally, the magnet is placed on top of the membrane, followed by curing the assembly under UV light for 90 seconds, allowing the photo initiator to polymerize the resin and create a strong bond between the magnet and the membrane. This efficient process allowed for the rapid production of 20 membranes in 15 minutes, showcasing the speed and precision of DLP printing.

Mechanical Characterization of The Electromagnetic Actuators

The goal of this experiment was to validate the operating principle of the actuator and to verify the vibration modes and operating (resonance) frequencies. Frequency response analysis was done using a non-destructive testing method, 3D scanning vibrometer (PSV-500 Scanning Vibrometer, Polytech, Germany) at the center of the membrane at steady state.

The experimental setup consisted of an electromagnetic actuator connected to an L293D half-H driver to produce an oscillating current at a desired frequency. Drivers were controlled with an Arduino Uno microcontroller and DC power supply. A 3D vibrometer PSV-500, a computer interface with analysis software, and anti-vibrating table (surface isolated from any external forces). Vibrations in the actuator were generated by electrical signal varying from 4 to 11 V DC. Additionally, a mechanical Bode plot of the actuators was obtained by driving it directly from the internal function generator of the PSV-500 (20 V peak to peak).

Electrical Characterization of The Electromagnetic Actuators

The electrical characterization of the electromagnetic actuator was performed using a Tektronix Oscilloscope Series 5. Two experimental setups were employed, both operating at a frequency of 200 Hz. In the first setup, a rectangular wave generated by the L293D half-H driver, powered by a DC power supply, was used to drive the actuator. The current flowing through the coil was measured, and the maximum input power was calculated, while the DC input voltage was varied between 4 and 11 V. In the second setup, the actuator was connected to a function generator, providing a sinusoidal wave at 200 Hz, and the maximum voltage (V_{max}) was swept from 4 to 10 V. These experiments allowed for a

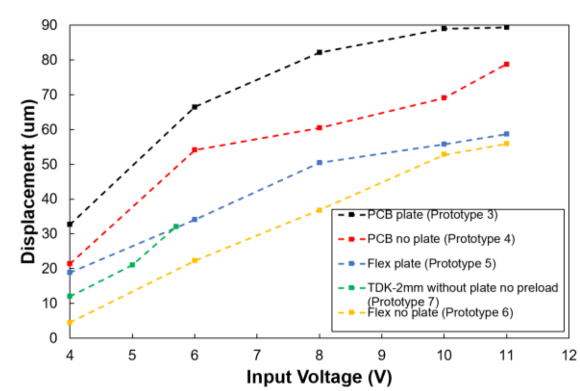

Figure 2: Mechanical characterization (maximum displacement) of the different actuators.

comprehensive analysis of the actuator's electrical behavior under different conditions.

RESULTS

Mechanical Analysis

The mechanical characterization studies the displacement and force output of the actuators under varying preload masses and input voltages, providing insights into the design's effectiveness for vibrotactile stimulation. Fig. 2 shows the mechanical characterization (maximum displacement) of the different actuators.

Prototypes 1 and 2 employed flexible-x resin as the flexible material, characterized by a Young's modulus of 2.4 MPa. The outer layer of these prototypes was fabricated using hard resin (Clear Impact from Liqcreate), a material with enhanced mechanical properties which served to securely fix the membrane to the coil, providing a stable and durable connection. These 2 prototypes used a rigid 12-layer Flexar PCB coil. The maximum displacement at the center of the membrane was observed to vary between 11 µm and 25 µm, contingent upon the presence or absence of a steel plate on the back of the coil. This indicates a significant influence of the steel plate on the actuator's performance, due to its concentration of the magnetic field, to further enhance its intensity. Actuator thickness increases from 2.6 mm to 3.6 mm with the back steel plate.

Initial prototypes 1 and 2 were iterated to increase the maximum displacement by changing the resin, which was supported by calculations from the second order mathematical model, where decreasing the Young's modulus will result in an increase in the displacement. Accordingly, prototypes 3 and 4 were fabricated with a new resin featuring a Young's modulus of 1.9 MPa, yielding a maximum displacement range of 11-90 µm which is sufficient for vibrotactile stimulation on fingers [18].

To further improve the dimensions and the flexibility of the actuator, prototypes 5 and 6 were fabricated and characterized at different input voltages. For these prototypes, a one-layer Flexar coil is used. The maximum displacement for these prototypes ranged from 4.5-59 µm, marking a significant reduction in the thickness while maintaining performance. This advancement brings the actuator closer to realizing a flexible wearable device capable of providing effective vibrotactile stimulation. The actuator thickness increases from 1.26 mm to 3.36 mm with the back steel plate.

Finally, prototype 7 was fabricated using only flexible material and TDK coils, resulting in a significant reduction in dimensions due to the coil size. This prototype achieved a maximum displacement range of 12-47 µm, further optimizing the design.

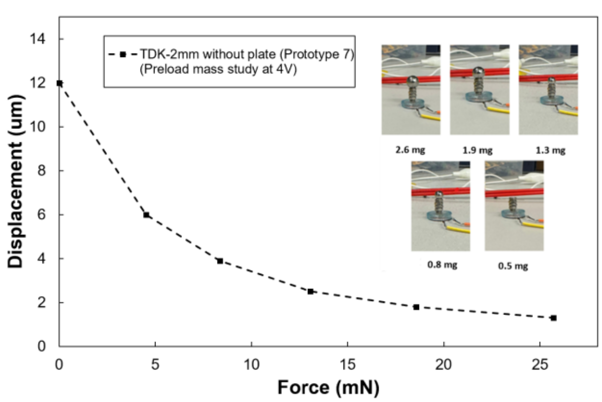

Figure 3: Mechanical characterization (laser vibrometer) with a change of preload mass. All samples excited at 4V. (inset) masses used to apply the preload force.

The study of the effect of preload mass on the actuator's performance is crucial because it enables the understanding of how the actuator will behave in various scenarios, particularly in applications where it will interact with human skin or other materials. For that purpose, a study was conducted on prototype 7 to investigate the effect of preload mass on the actuator's performance. Spherical steel masses of varying weights ($m = F/g$) were placed on top of the actuator, generating a preload force between 4-26 mN, which is the minimum indentation force required for human skin sensation. This resulted in a displacement range of 1.5-12 µm, as shown in Fig. 3.

To analyze the dynamic behavior, a bode plot was measured using the internal function generator of the laser vibrometer (sweep mode at 20 V peak to peak) for prototype 7 (Fig. 5), enabling the extraction of a lumped element model. The dimensions of this prototype were 12 mm × 12 mm × 2.8 mm. A comparison between the mathematical model and the bode plot experimental results is shown in Fig. 4, showing a natural frequency of 48 Hz. The Lumped Element Model (LEM) is shown in Fig. 4 (inset) and is composed of two separate domains: the electrical domain and the mechanical domain. In the electrical domain, the coil's resistance (R_{coil}) and inductance (L_{coil}) combine to form the electrical impedance. The mechanical behavior is simplified to a mass-spring-damper model. The overall mass (m_m) includes the mass of the magnet and the printed membrane. The total compliance (C_m) represents the inverse of the mechanical stiffness of the membrane, while the damping coefficient (b) accounts for mechanical losses.

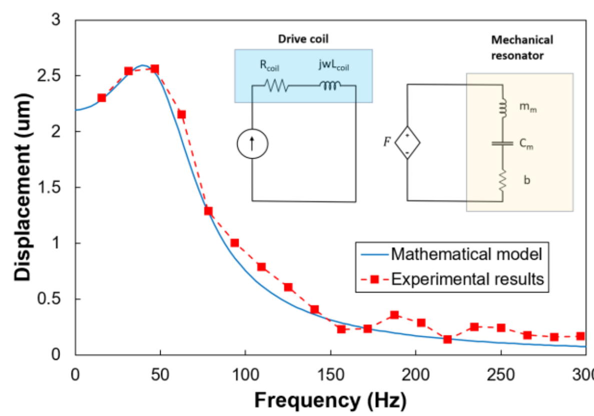

Figure 4: Mathematical model and bode plot experimental results comparison (Prototype 7).

Electrical Analysis

The power consumption of the actuators was thoroughly evaluated using oscilloscope measurements, and the results are presented in Fig. 5. To assess the maximum input power, the three different coils used in the different prototypes were tested using both sinusoidal and square waveforms at a frequency of 200 Hz. The results show a significant reduction in maximum power consumption when using a sinusoidal waveform, with values ranging from 50-340 mW, compared to 380-5325 mW when using a square waveform. However, when examining the average input power, a different trend emerged. The rectangular waveform exhibited an average input power of 10-138 mW, which is attributed to the pulses of current with a peak current varying between 100 and 450 mA at 200 Hz. This suggests that while sinusoidal waveforms are more power-efficient in terms of maximum input power, the rectangular waveform's pulsing nature results in a lower average power consumption.

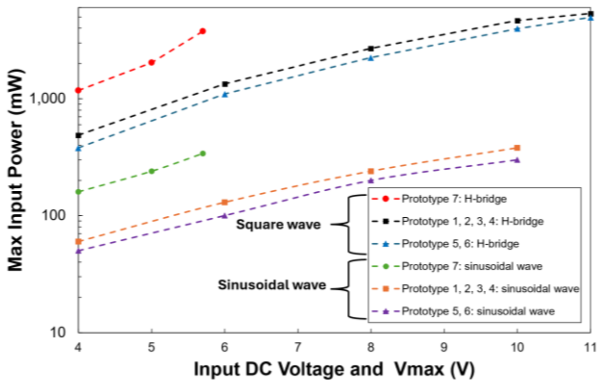

Figure 5: Electrical characterization (oscilloscope) of different coils showing maximum power input change. Measurements were done for sinusoidal and square waves using an L293D half-H drivers.

CONCLUSIONS

In conclusion, this paper presents a novel approach to soft electromagnetic haptic actuators, leveraging DLP multimaterial 3D printing, off-the-shelf magnets, and planar coils. The proposed actuators offer a promising solution for wearable haptic devices in VR/AR platforms, providing high performance with high out-of-plane displacement, low power consumption, and ease of integration with compact design. Prototype 7, consisting of a TDK coil, flexible membrane, and a cylindrical magnet, was evaluated to be the optimal design among all actuators, exhibiting high performance with a maximum out-of-plane displacement range of 12-47 µm, sufficient for vibrotactile stimulation on fingers, low power consumption with a maximum input power of 160-340 mW at 200 Hz (resonance), ease of integration with a compact design and dimensions as small as 12 x 12 x 2.8 mm enabling wearable devices. The study of preload mass effects and electrical characterization provides valuable insights into the actuators' behavior and optimization, paving the way for further research and development of soft haptic actuators. These findings demonstrate the potential of the proposed actuators for wearable haptic applications and lay the groundwork for further research and development in this field, enabling more immersive and interactive experiences in VR/AR and beyond. Ultimately, the development of high-performance, compact, and energy efficient haptic actuators is crucial for unlocking the full potential of haptic technology, allowing users to feel tactile sensations and feedback in real time, and creating a more natural and intuitive interface between humans and machines.

ACKNOWLEDGEMENTS

The authors gratefully acknowledge funding support from the Reality Labs Research, Meta Platforms Inc, and the National Institutes of Health for the Laser Scanning Vibrometer grant, NIH S10OD032194. We also thank the students from the Magnetic, Microsystems, & Microrobotics lab for their contribution.

REFERENCES

[1] X. Zhang, Y. Chen, L. Hu, and Y. Wang. "The metaverse in education: Definition, framework, features, potential applications, challenges, and future research topics", *Frontiers in Psychology* 13 (2022): 1016300.

[2] K. Song, S. Kim, and Y. Cha. "Soft electromagnetic actuator for assembly robots", *Smart Materials and Structures* 29, no. 6 (2020): 067001.

[3] X. Yu, Z. Xie, Y. Yu, J. Lee, A.V. Guardado, H. Luan, J. Ruban et al. "Skin-integrated wireless haptic interfaces for virtual and augmented reality", *Nature* 575, no. 7783 (2019): 473-479.

[4] W. Dangxiao, G. U. O. Yuan, L. I. U. Shiyi, Y. Zhang, X. Weiliang, and X. Jing. "Haptic display for virtual reality: progress and challenges", *Virtual Reality & Intelligent Hardware* 1, no. 2 (2019): 136-162.

[5] R. Hinchet, V. Vechev, H. Shea, and O. Hilliges. "Dextres: Wearable haptic feedback for grasping in VR via a thin form-factor electrostatic brake", In *Proceedings of the 31st Annual ACM Symposium on User Interface Software and Technology*, pp. 901-912. (2018).

[6] X. Ji, X. Liu, V. Cacucciolo, Y. Civet, A. E. Haitami, S. Cantin, Y. Perriard, and H. Shea. "Untethered feel-through haptics using 18-µm thick dielectric elastomer actuators", *Advanced Functional Materials* 31, no. 39 (2021): 2006639.

[7] C. H. Yeh, F. C. Su, Y. S. Shan, M. Dosaev, Y. Selyutskiy, I. Goryacheva, and M. S. Ju. "Application of piezoelectric actuator to simplified haptic feedback system", *Sensors and Actuators A: Physical* 303 (2020): 111820.

[8] J. Mu, M. J. Andrade, S. Fang, X. Wang, E. Gao, N. Li, S. H. Kim et al. "Sheath-run artificial muscles", *Science* 365, no. 6449 (2019): 150-155.

[9] X. Tang, H. Li, T. Ma, Y. Yang, J. Luo, H. Wang, and P. Jiang. "A review of soft actuator motion: Actuation, design, manufacturing and applications", In *Actuators*, vol. 11, no. 11, p. 331. MDPI, (2022).

[10] A. P. Taylor, C. Cuervo, D. P. Arnold, and L. F. Velásquez-García. "Fully 3D-printed, monolithic, mini magnetic actuators for low-cost, compact systems", *Journal of Microelectromechanical Systems* 28, no. 3 (2019): 481-493.

[11] E. Acome, S. K. Mitchell, T. G. Morrissey, M. B. Emmett, C. Benjamin, M. King, M. Radakovitz, and C. Keplinger. "Hydraulically amplified self-healing electrostatic actuators with muscle-like performance", *Science* 359, no. 6371 (2018): 61-65.

[12] G. Mao, M. Drack, M. K. Mosammam, D. Wirthl, T. Stockinger, R. Schwödiauer, and M. Kaltenbrunner. "Soft electromagnetic actuators", *Science advances* 6, no. 26 (2020): eabc0251.

[13] S. A. Morin., R. F. Shepherd, S. W. Kwok, A. A. Stokes, A. Nemiroski, and G. M. Whitesides. "Camouflage and display for soft machines", *Science* 337, no. 6096 (2012): 828-832.

[14] P. Polygerinos, Z. Wang, K. C. Galloway, R. J. Wood, and C. J. Walsh. "Soft robotic glove for combined assistance and at-home rehabilitation", *Robotics and Autonomous Systems* 73 (2015): 135-143.

[15] V. Vechev, J. Zarate, D. Lindlbauer, R. Hinchet, H. Shea, and O. Hilliges. "Tactiles: Dual-mode low-power electromagnetic actuators for rendering continuous contact and spatial haptic patterns in VR", In *2019 IEEE Conference on Virtual Reality and 3D User Interfaces (VR)*, pp. 312-320. IEEE, (2019).

[16] R. John, F. J. Milford, R. W. Christy, S. Kunde, and S. Hermiston. "Foundations of electromagnetic theory", (1967).

[17] H. L. Yin, Y. C. Huang, W. Fang, and J. Hsieh. "A novel electromagnetic elastomer membrane actuator with a semi-embedded coil", *Sensors and Actuators A: Physical* 139, no. 1-2 (2007): 194-202.

[18] J. Yin, R. Hinchet, H. Shea, and C. Majidi. "Wearable soft technologies for haptic sensing and feedback", *Advanced Functional Materials* 31, no. 39 (2021): 2007428.

CONTACT

* N. Tarabay, +1-949-691-2642; ntarabay@uci.edu
* C. Velez, +1-352-575-7581; cvelezcu@uci.edu